Bone Reports 17 (2022) 101621

Contents lists available at ScienceDirect

Bone Reports

journal homepage: www.elsevier.com/locate/bonr

Deletion of osteopontin or bone sialoprotein induces opposite bone responses to mechanical stimulation in mice

M. Maalouf [a,*], H. Çinar [a], W. Bouleftour [b], M. Thomas [a], A. Vanden-Bossche [a], N. Laroche [a], M.T. Linossier [a], S. Peyroche [a], M.H. Lafage-Proust [a], L. Vico [a], A. Guignandon [a], L. Malaval [a]

[a] LBTO, INSERM, U1059-SAINBIOSE, Université de Lyon, Université Jean Monnet, Saint-Etienne, France
[b] Hôpital Nord, University Hospital, Université Jean Monnet, Saint-Etienne, France

ARTICLE INFO

Keywords:
Hypergravity
Whole body vibration
Osteopontin
Bone sialoprotein
Knockout

ABSTRACT

Osteopontin (OPN) and Bone Sialoprotein (BSP) are co-expressed in bone and display overlapping and complementary physiological properties. Both genes show a rapid expression response to mechanical stimulation. We used mice with single and double deletions (DKO) of BSP and OPN to assess the specificity of their roles in skeletal adaptation to loading. Two-month-old Wild-Type (WT), BSP knockout ($BSP^{-/-}$), $OPN^{-/-}$ and DKO male mice were submitted to two mechanical stimulation regimen (n = 10 mice/group) respectively impacting trabecular bone (Hypergravity, HG) and cortical bone (Whole Body Vibration, WBV). HG increased trabecular bone volume (BV/TV) in WT femur through reduced resorption, and in $BSP^{-/-}$ mice femur and vertebra through increased bone formation. In contrast, HG increased the turnover of $OPN^{-/-}$ bone, resulting in reduced femur and vertebra BV/TV. HG did not affect DKO bones. Similarly, WBV increased cortical thickness in $BSP^{-/-}$ mice and decreased it in $OPN^{-/-}$, without affecting structurally WT and DKO bone. Vibrated $BSP^{-/-}$ mice displayed increased endocortical bone formation with a drop in Sclerostin expression, and reduced periosteal osteoclasts with lower Rankl and Cathepsin K expression. In contrast, vibrated $OPN^{-/-}$ endocortical bone displayed decreased formation and increased osteoclast coverage. Therefore, under two regimen (HG and WBV) targeting distinct bone compartments, absence of OPN resulted in bone loss while lack of BSP induced bone gain, reflecting divergent structural adaptations. Strikingly, absence of both proteins led to a relative insensitivity to either mechanical challenge. Interplay between OPN and BSP thus appears as a key element of skeletal response to mechanical stimulation.

1. Introduction

Osteopontin (OPN) and Bone Sialoprotein (BSP) are two non-collagenous proteins present in the bone matrix and involved in bone formation, resorption and mineralization processes (Ganss et al., 1999; Sodek et al., 2000). Together with Matrix Extracellular Phosphoglycoprotein (MEPE), Dentin Matrix Protein-1 (DMP1) and Dentin Sialophosphoprotein (DSPP), OPN and BSP form the SIBLING (Small Integrin Binding Ligand N-linked Glycoproteins), a family of phylogenetically related extracellular matrix components whose genes are aligned on the same chromosome (4 in human, 5 in mouse) (Fisher and Fedarko, 2003; Staines et al., 2012). In a 129sv/CD1 mouse genetic background (wild-type, WT) single gene knockouts of BSP ($BSP^{-/-}$, (Malaval et al., 2008)), OPN ($OPN^{-/-}$), as well as a double knockout ($BSP^{-/-} + OPN^{-/-} = DKO$, (Bouleftour et al., 2019)) have been developed and/or characterized in our group. We generated DKO mice because of the evidence of a functional compensation between BSP and OPN in the anabolic bone response to Parathyroid Hormone (PTH) (Bouleftour et al., 2015) and because $BSP^{-/-}$ mice over-express OPN protein in bone tissue and in blood (Granito et al., 2015). Interestingly, all three genetic conditions ($BSP^{-/-}$, $OPN^{-/-}$ and DKO) affect trabecular and cortical bone architecture and dynamics in distinct ways (Bouleftour et al., 2019).

* Corresponding author at: LBTO, INSERM, U1059-SAINBIOSE, Université de Lyon - Université Jean Monnet, Pôle Santé Nord - Faculté de Médecine, Rm 118, 10 Chemin de la Marandière, F 42270 St Priest en Jarez, France.

E-mail addresses: mathieu.maalouf@univ-st-etienne.fr (M. Maalouf), Wafa.Esquis@chu-st-etienne.fr (W. Bouleftour), mireille.thomas@univ-st-etienne.fr (M. Thomas), arnaud.vanden.bossche@univ-st-etienne.fr (A. Vanden-Bossche), norbert.laroche@univ-st-etienne.fr (N. Laroche), linossier@univ-st-etienne.fr (M.T. Linossier), sylvie.peyroche@univ-st-etienne.fr (S. Peyroche), MH.Lafage.Proust@univ-st-etienne.fr (M.H. Lafage-Proust), vico@univ-st-etienne.fr (L. Vico), alain.guignandon@univ-st-etienne.fr (A. Guignandon), luc.malaval@univ-st-etienne.fr (L. Malaval).

https://doi.org/10.1016/j.bonr.2022.101621
Received 3 September 2022; Received in revised form 14 September 2022; Accepted 16 September 2022
Available online 17 September 2022

OPN and BSP have been shown in many in vitro and in vivo models to be rapidly and temporarily (hours or days) expressed by bone cells in response to mechanical stimulation (Kreke et al., 2005; Mitsui et al., 2005; Terai et al., 1999; Yu et al., 2009; Zhou et al., 2015), which makes them early markers of bone's perception of loading. To our knowledge, only one study reported the effect of increased mechanical loading on $OPN^{-/-}$ mice and showed in calvaria sutures a delay in formation activity under tensile mechanical stress (Morinobu et al., 2003). No study to date has investigated the effects of loading on other bone compartments of $OPN^{-/-}$, $BSP^{-/-}$ or DKO mice. To evaluate the role of these proteins and their interactions under mechanical challenge, we tested WT, $BSP^{-/-}$, $OPN^{-/-}$ and DKO mice in two different mechanical stimulation challenges: hypergravity (HG) and whole body vibration (WBV). Our laboratory has previously described the impact of HG and WBV on the skeleton of seven-week-old C57Bl/6 mice. In these studies, each challenge displayed structural effects targeting a specific bone compartment. Under a 2G acceleration, HG increased trabecular bone mass (Gnyubkin et al., 2015) whereas WBV (at 2G and 90 Hz) accelerated cortical bone accrual (Gnyubkin et al., 2016). In the present study, this compartment specificity allowed us to assess the impact of mechanical stimulation on mice with mutations affecting both trabecular and cortical bone (Bouleftour et al., 2019).

Since OPN and BSP exhibit overlapping and complementary bone physiological properties and both genes are rapidly overexpressed under mechanical stress, we hypothesized that these proteins may have critical and interactive roles in the skeletal response to mechanical stress.

2. Materials & methods

2.1. Animal care

WT 129sv/CD1 mice, along with $BSP^{-/-}$, $OPN^{-/-}$ and DKO mice in the same genetic background were used in these experiments. $BSP^{-/-}$ mice have been generated by homologous recombination, as described (Malaval et al., 2008). $OPN^{-/-}$ and DKO mice were engineered through targeted deletion, using the Transcription Activator-Like Effector Nuclease (TALEN) technique on a $BSP^{+/-}$ background, as described (Bouleftour et al., 2019). For line maintenance and experimentation, the animals were housed and bred in the PLEXAN facility (Platform for Experiments and Analysis, Faculty of Medicine, University Jean Monnet, Saint-Etienne, France). Mice were kept at standard temperature (23 ± 2 °C), in a light-controlled environment (12 h light/12 h dark cycle) and were fed a standard pellet diet (SAFE A03, Safe, Augy, France) with water ad libitum. All animal experiments have been approved by the local ethical committee (Comité d'Ethique en Experimentation Animale de la Loire CEEAL-UJM, agreement Nr°98) and the Animal Welfare Committee of the PLEXAN. After screening by the CEEAL-UJM, HG experiments received approval from the national authority (Ministère de l'Enseignement Supérieur, de la Recherche et de l'Innovation, APAFIS Nr 8160-2016112415129882 v6). The procedures for the care and euthanizing of the animals were in accordance with the European Community Standards on the care and use of laboratory animals (Ministère de l'Agriculture, France, Authorization Nr°42-18-0801).

2.2. Hypergravity regimen

The 1.4 m radius centrifuge with four peripheral gondolas associated with an electronic control system (COMAT Aérospace, Flourens, France) is housed in the PLEXAN site ((Gnyubkin et al., 2015), Fig. 1A). All gondolas are equipped with a camera-based monitoring system to track the behavior of the animals and the food/water stocks (Fig. 1B). Two-month-old male mice of all 4 genotypes were separated between controls, kept at normal gravity (1G), and a centrifuged group (2G) (n = 10 mice/genotype/group). Cages of the 2G groups were transferred into the gondolas (10 mice/cage/gondola, Fig. 1B) and the centrifuge was run at 2G acceleration for 3 weeks, with a weekly 5-min stop to weigh the mice and renew food and water. Control cages were kept in the centrifuge room to homogenize environmental factors.

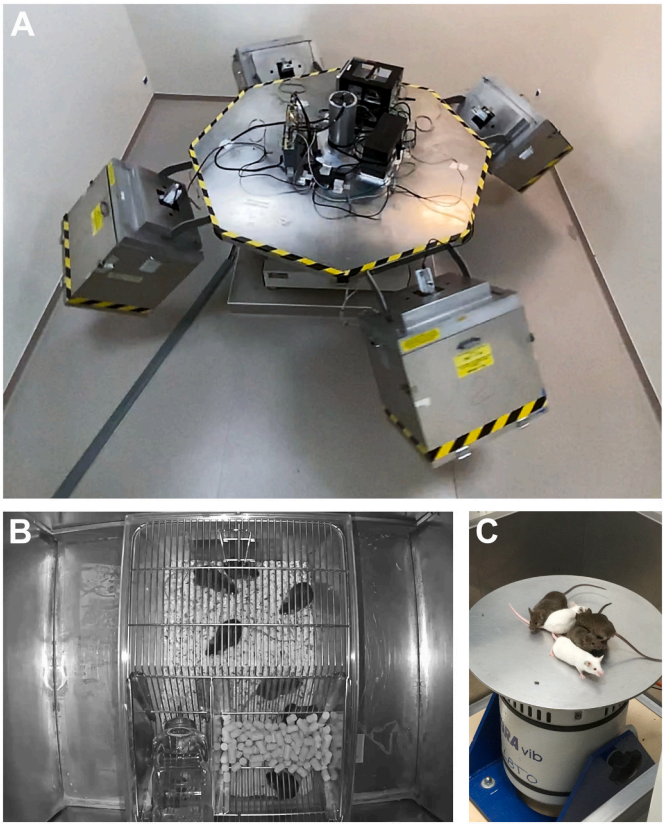

Fig. 1. Hypergravity and whole body vibration apparatus used for mechanical stimulation on mice. (A) For hypergravity experiment the centrifuge is composed of a central disc and four arms holding peripheral swinging gondolas. (B) The gondolas are designed to hold rodent cages and are equipped with a video monitoring system. (C) For whole body vibration experiments, the mice are placed on an aluminum disk that is attached to a shaker platform during the vibration session.

2.3. Whole body vibration regimen

Shaker platforms (TIRA Vibration Test Systems TV 52120, Schalkau, Germany) on which aluminum discs (30 cm diameter, 4 mm thickness) are attached were used to generate vibrations ((Gnyubkin et al., 2016), Fig. 1C). The G-level was controlled by an accelerometer (PBB Piezotronics, 100 mV/g, ref. 352C33). Two-month-old male mice of all 4 genotypes were separated between controls (CT) and vibrated (VB) (n = 10 mice/genotype/group). During each WBV session, all mice from the same cage were put on the shaker's disc and left free to move (Fig. 1C). For VB mice, the plates were accelerated at 2G, at a 90 Hz frequency (sinusoidal signal) for 15 min/day, 5 day/week (Monday to Friday) during 6 weeks. CT mice were put on an inactive shaker for 15 min during the vibration sessions, alternating with the VB.

2.4. Tetracycline labelling and sample collection

In order to label bone formation surfaces, all mice were injected with 30 mg/kg tetracycline (TTC, Sigma-Aldrich) in saline solution, seven days and three days before euthanasia. At the respective ends of HG and WBV experiments, all mice were euthanized and femora, vertebrae and tibiae were collected.

2.5. Microtomography

For microtomographic (μCT) analysis, formalin-fixed and ethanol dehydrated femur and second lumbar (L2) vertebra were scanned with a Viva CT40 tomograph (Scanco Medical, Bassersdorf, Switzerland) following standard guidelines (Bouxsein et al., 2010). Data were acquired at 55 keV with a 145 mA current and a 10 μm isotropic voxel size. Three-dimensional reconstructions were generated using the following parameters: σ = 1.2; support = 2; threshold = 245 for trabecular bone and 280 for cortical bone.

The structural parameters of trabecular bone, bone volume/trabecular volume (BV/TV), trabecular thickness (Tb.Th), trabecular number (Tb.N), trabecular separation (Tb.Sp), structure model index (SMI) and density of connections (Conn.D) were measured in a set of 150 sections above the distal growth plate of the femur and from all sections between the two growth plates of the L2 vertebra. Measurements were done within Regions of Interest (ROI) excluding primary trabecular bone and cortical bone, which had been manually defined by the same operator on transversal 2D images. The structural parameters of the femur midshaft, cortical thickness (Ct.Th), total cross sectional area (Tt.Ar), cortical area (Ct.Ar), marrow area (Ma.Ar), cortical porosity (Ct.Po), maximal (Imax) and minimal areal moment of inertia (Imin), polar moment of inertia (pMOI = Imax + Imin), maximal radius perpendicular to Imax direction (Cmax), minimal radius perpendicular to Imin direction (Cmin), section module (Imax/Cmax and Imin/Cmin) and tissue mineral density (TMD), as calibrated with an HAP phantom, were calculated by integration of the value on each transverse section of a set of 60, starting 500 sections (5 mm) above the distal growth plate. ROI for cortical bone were automatically contoured using an edge detection software tool. On the 30th section of each image stack, the cortical bone was compartmentalized into radial sectors separated by 45 degrees and the cortical thickness was manually measured in each sector with the μCT software.

2.6. Histomorphometry

After μCT analysis, femur bones were cut in two with a Dremel model 395 electric drill fitted with a diamond blade (Dremel Multipro, Breda, Netherlands) at the lower two-thirds of their length. Both parts were embedded separately in methyl-methacrylate.

The distal metaphysis was cut longitudinally with a tungsten-carbide-bladed microtome (Leica SM2500E, Wetzlar, Germany) to obtain 9 μm slices. Sections were stained with modified Goldner's trichrome or with tartrate-resistant acid phosphatase (TRAcP) histochemistry for osteoclasts with Light-Green counterstain, or were left unstained. Bone formation was assessed on unstained sections by measuring single (sLs/BS) and double TTC labeled surfaces per bone surface (dLs/BS) and derive mineralizing surfaces per bone surface (MS/BS, in %, with MS = 0.5*sLs + dLs). The mineral apposition rate (MAR, in μm/day) was assessed as the distance between double labels. The bone formation rate per bone surface (BFR/BS, in $\mu m^3/\mu m^2$/day) was calculated as (MS/BS)*MAR. Osteoclast surfaces per bone surface (Oc.S/BS, in %), osteoclast number per bone perimeter (N.Oc/B·Pm) and osteoclast mean length (Oc.Le) were measured on TRAcP stained sections. Measurements excluded primary bone to fit with the ROI of μCT analysis. Results for each mouse are averages of 5 non-successive sections. Femur midshaft was cut transversely with a diamond-coated wire (Escil, Precision Diamond Wire Saw, Chassieu, France) into 300 μm slices. The bone formation parameters, mineralized perimeter per bone perimeter (MPm/BPm, in %), MAR and BFR per bone perimeter (BFR/BPm, $\mu m^2/\mu m$/d) were measured on one slice per mouse, taken within the μCT ROI. Measurements were made on the unstained and unmounted section, kept flat on a slide in a few drops of alcohol during analysis. The section was then gradually rehydrated, TRAcP-stained without counter-staining, mounted and re-analyzed for osteoclast perimeter per bone perimeter (Oc.Pm/BPm, %). Measurements were done on endocortical (Ec.) and periosteal surfaces (Ps.) separately, and on both sides of each slice, whose values were averaged.

2.7. Real-Time PCR

For quantitative real-time PCR analysis (RT-qPCR) of WBV cortical bone, collected tibiae were cleaned from connective tissue, their shafts were cut-out and flushed with sterile PBS to restrict the sampling to cortical bone, then crushed in liquid nitrogen with steel balls in a mixer mill (Sartorius, Gottingen, Germany) before extraction with Tri-Reagent (Sigma-Aldrich). For HG experiment, the tibia shafts were flushed with Tri-Reagent in order to best sample the trabecular compartment. RNA harvested with Tri-Reagent was purified on columns (Rneasy Plus Mini Kit, Qiagen, Hilden, Germany), quantified with the Ribogreen kit (Invitrogen, Life Technologies, Eugene, OR, USA) and quality checked with an Experion automated electrophoresis station (Bio Rad, Hercules, CA, USA). Messenger RNA was reverse transcribed (iScript cDNA synthesis Kit, Biorad) and 400 ng of cDNA were amplified using the SYBR Green I dye (Lightcycler faststart DNA masterSYBR green I, Roche, Germany). Names and primer sequences of the genes of interest are given in Table S1. Expression of the housekeeping gene glyceraldehyde-3-phosphate dehydrogenase (GAPDH) did not vary significantly within or between groups (not shown).

2.8. Statistics

The conditions of normality (Shapiro-Francia test) and homoscedasticity (equality of variances, F-test) were verified only in a subset of our data, to which Fisher's *t*-test could therefore be applied for intergroup comparisons (Figs. 2C, 4B, vertebrae in Table S2). The non-parametric Wilcoxon-Mann-Whitney *U* test was used for the rest (Figs. 2, 3, 4A and 5, femora in Tables S2, S3, S4 and S5). Analysis of variance was not used as it demands normality and homoscedasticity of the data, and because the phenotypes of the different mutant lines are independent from each other. We did not adjust for multiple hypotheses testing given the exploratory character of this study, whose goal is to draw a picture of phenotypic adjustment to mechanical signals in the four mouse genotypes.

3. Results

3.1. Hypergravity induces trabecular bone loss in $OPN^{-/-}$ mice, in contrast to bone gain in WT and $BSP^{-/-}$ mice

Only WT mice showed a (~10 %) reduction of their final weight under HG (Table S2). At 2G, WT and $BSP^{-/-}$ mice increased their trabecular BV/TV (+27 % for both, Fig. 2B) and Tb.Th (+11 % for WT and + 9 % for $BSP^{-/-}$, Fig. 2D) in the distal femoral metaphysis with the addition of an increase of Conn.D only for $BSP^{-/-}$ mice (+23 %, Fig. 2E). Strikingly, $OPN^{-/-}$ mice lost femoral trabecular BV/TV (−27 %) and Conn.D (−20 %) under HG, with no change for the DKO (Fig. 2B, D, E). Similar effects of HG were observed in L2 vertebra for all genotypes except the WT, which showed no bone gain under HG, highlighting the greater overall response of $BSP^{-/-}$ mice (Fig. 2C, Table S2). No effect of HG on cortical parameters was observed for any genotype (Table S2).

3.2. Hypergravity effects on bone cellular activities are genotype-specific

In WT trabecular bone, HG decreased significantly Oc.S/BS with no significant change in BFR/BS (Fig. 3A, C). Nonetheless, RT-qPCR analysis of the tibial trabecular compartment of WT mice showed increased Osterix (OSX), Osteocalcin (OCN) and Alkaline phosphatase (ALP) expression under 2G (Fig. 3D, Table S3). HG increased trabecular bone remodeling in $OPN^{-/-}$ mice, with higher BFR/BS and Oc.S/BS (Fig. 3A, C) as well as increased OSX, ALP, OCN and TRAcP expression (Fig. 3D, Table S3). $BSP^{-/-}$ mice showed a specific increase in BFR/BS with no change in Oc.S/BS (Fig. 3A, B) with an increased expression of Estrogen

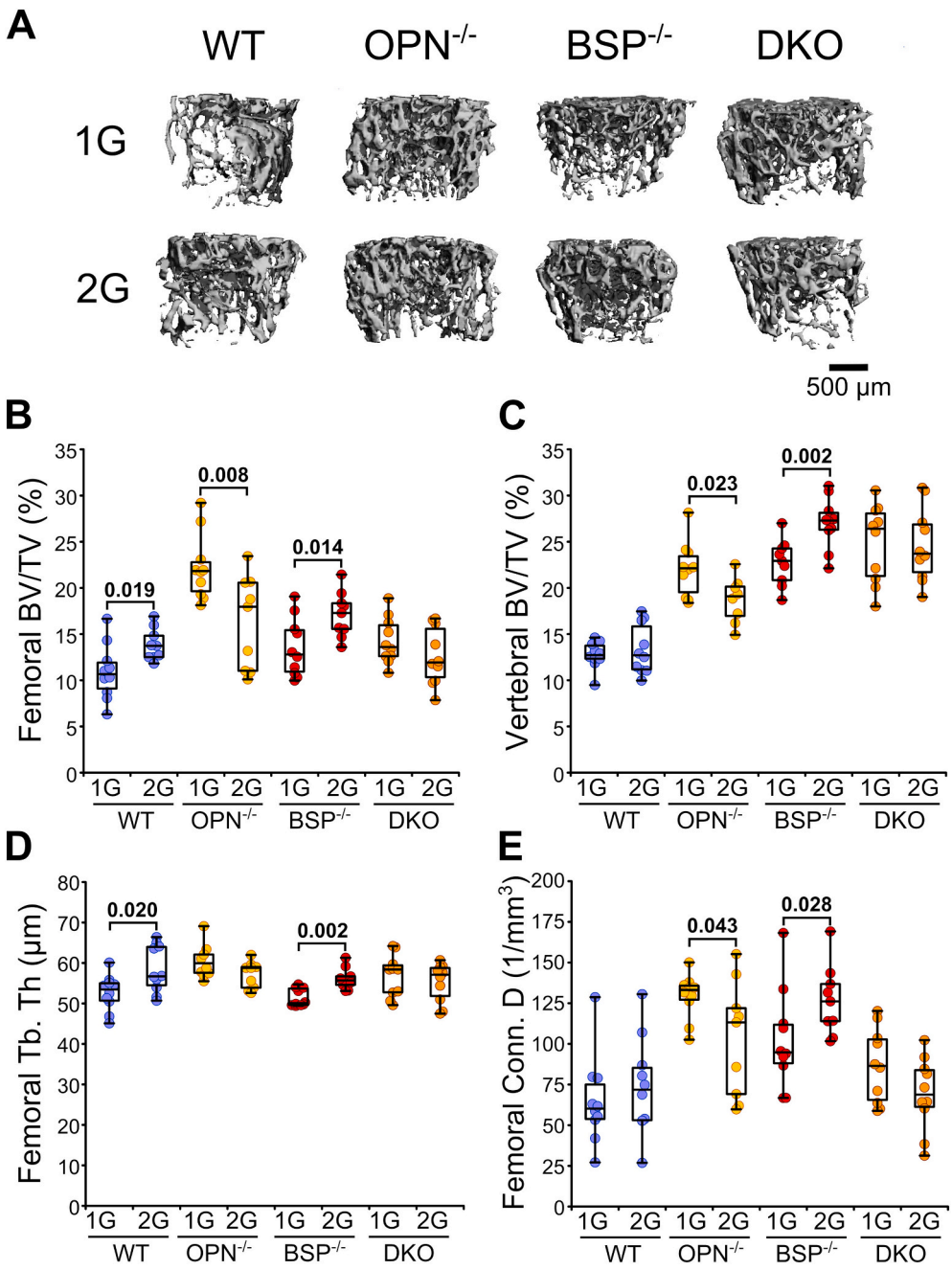

Fig. 2. Effect of 2G hypergravity on the trabecular bone of the femoral distal metaphysis and the L2-vertebra of WT, OPN$^{-/-}$, BSP$^{-/-}$ and DKO mice. (A) 3D reconstruction images of femoral trabecular bone. (B) Femoral and (C) vertebral BV/TV, (D) femoral Tb.Th and (E) Conn.D. The graph gives *p*-values between genotype-matched 1G and 2G, Fisher *t*-test (for C) or Mann-Whitney *U* test, N = 9–10 mice/group. See also Table S2.

receptor alpha (ERα) (Fig. 3D). DKO mice showed no significant change in bone cellular activity or mRNA expression under HG (Fig. 3A, D, Tables S2, S3).

3.3. *Whole body vibration induces cortical bone loss in OPN$^{-/-}$ mice, in contrast to bone gain in BSP$^{-/-}$ mice*

WBV did not affect body weight in any genotype (Table S4). No structural change was observed in the cortical bone of VB WT and DKO mice (Fig. 4, Table S4). VB OPN$^{-/-}$ mice displayed significant decrease of Ct.Th, Ct.Ar and Tt.Ar (−9 %, −13 % and −9 % respectively, Fig. 4A). In contrast, BSP$^{-/-}$ mice showed a significant increase in Ct.Th (+7 %) under WBV (Fig. 4A), with a trend towards a decrease of the Ma.Ar/Tt. Ar ratio (p = 0.061, Table S4) and no change in Tt.Ar (Fig. 4A), indicative of a narrowing medullary space under WBV. VB OPN$^{-/-}$ mice showed a reduction in pMOI (Fig. 4A), Imax/Cmax and Imin/Cmin (Table S4), reflecting a modification of bone mass distribution likely to impact biomechanical properties. The local cortical thicknesses analysis showed an uneven thinning of cortical bone in VB OPN$^{-/-}$ mice, mostly located in the anterolateral and posterolateral sectors, while cortical thickening in VB BSP$^{-/-}$ mice occurred in all sectors except the lateral (Fig. 4B).

Of note, OPN$^{-/-}$ was the only genotype to show a structural effect on trabecular bone under WBV, with a reduction of BV/TV (vertebra) and/or trabecular quality (smaller Tb.N, higher Tb.Sp, smaller Conn.D in VB femur, Table S4).

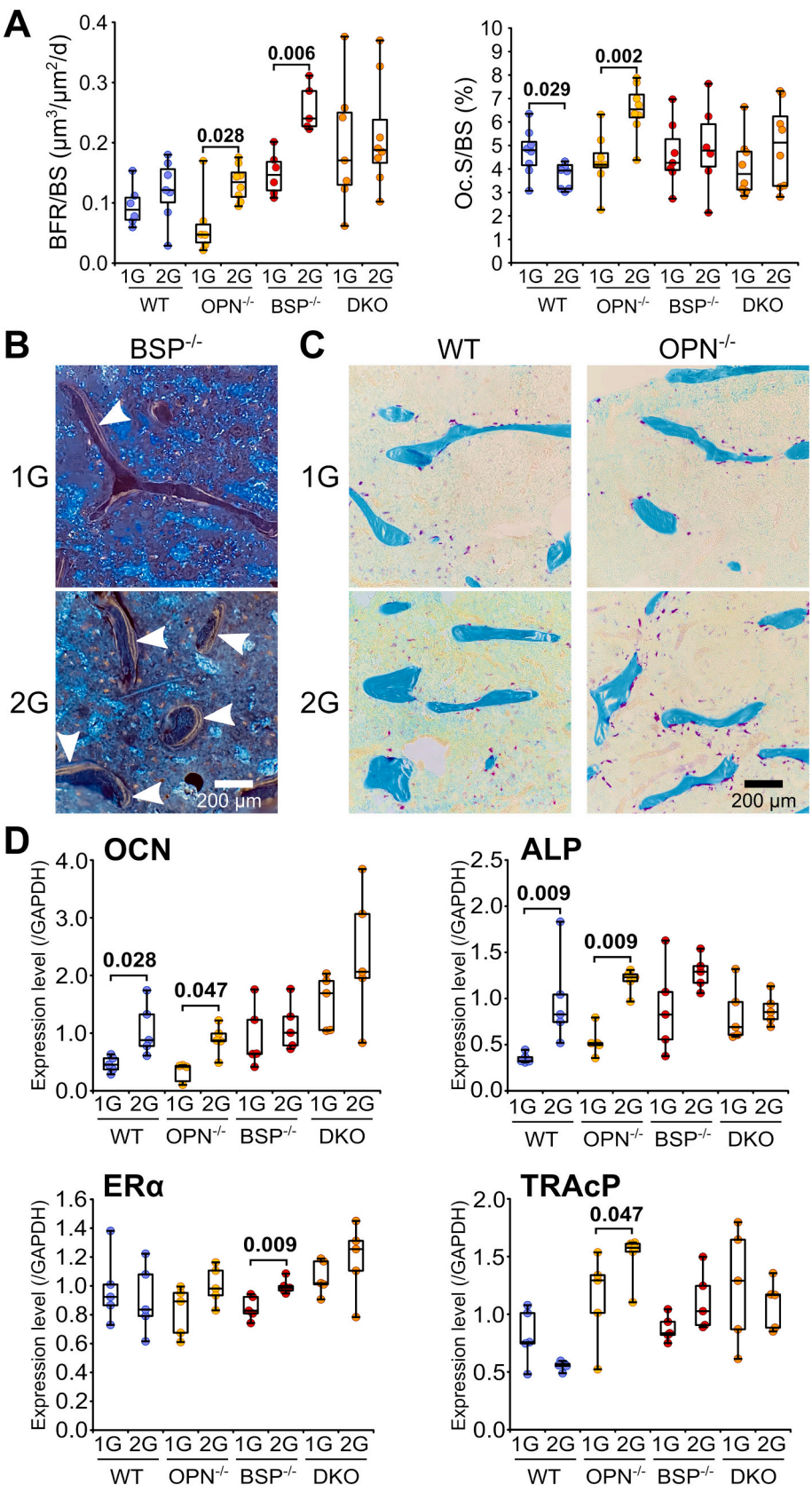

Fig. 3. Effect of 2G hypergravity on trabecular cellular activities and molecular markers in long bones of WT, OPN$^{-/-}$, BSP$^{-/-}$ and DKO mice. (A) Bone formation activity (BFR/BS) and osteoclast surfaces (Oc.S/BS), (B) Tetracyclin labelling and (C) TRAcP staining of the femur distal metaphysis at the end-point of the experiment, white arrows indicate trabecular double labeling surfaces in BSP$^{-/-}$ mice. (D) Marker mRNA expression in the tibial bone shaft, given as ratio to the housekeeping gene GAPDH. The graphs gives *p* values between genotype-matched 1G and 2G, Mann-Whitney U test, N = 5–10 mice/group. See also Tables S2 and S3.

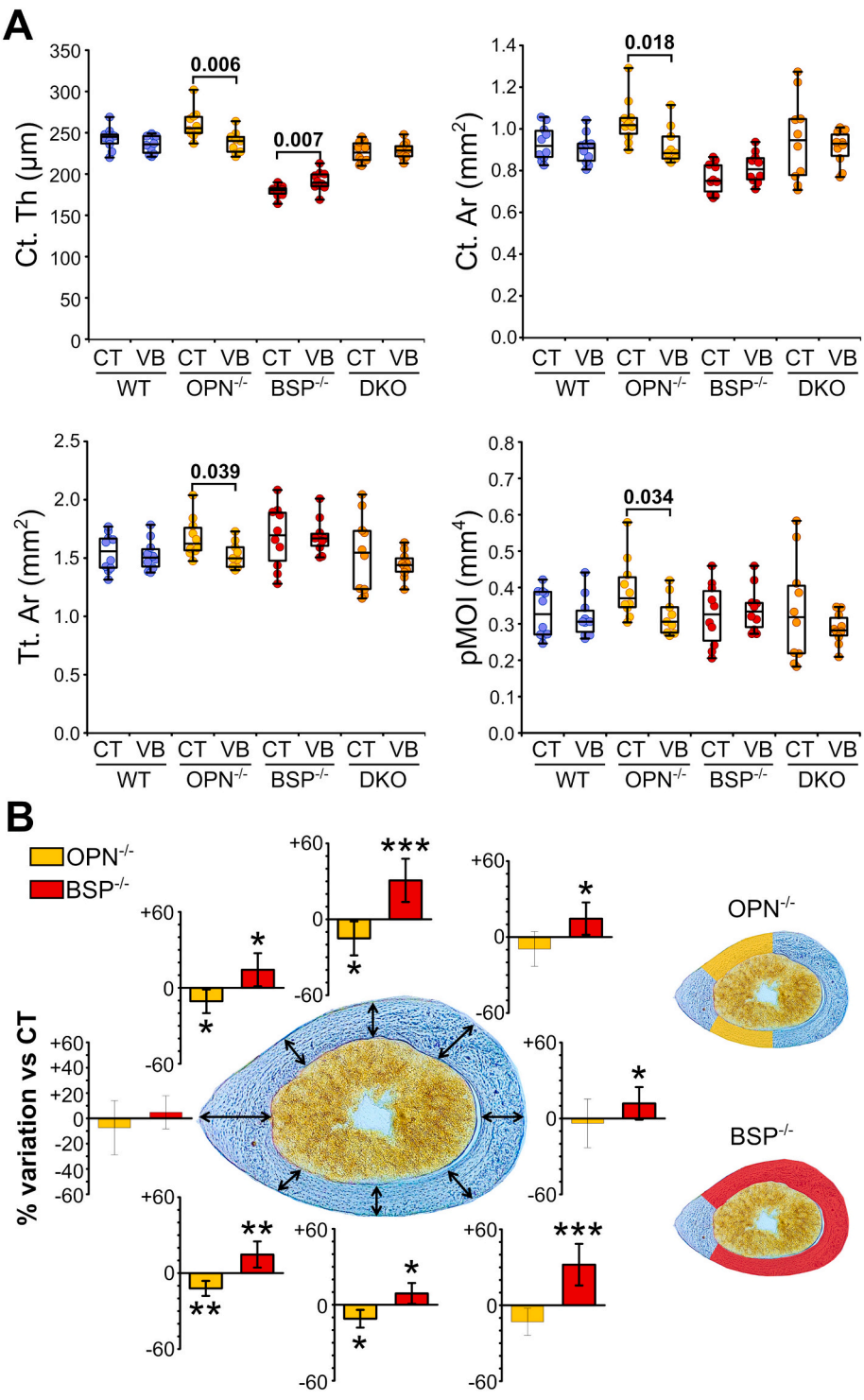

Fig. 4. Effect of WBV on the femoral cortical bone of WT, $OPN^{-/-}$, $BSP^{-/-}$ and DKO mice. (A) Cortical thickness (Ct.Th), cortical area (Ct.Ar), total area (Tt. Ar) and polar moment of inertia (pMOI) of control (CT) and vibrated (VB) mice. The graph gives p-values between genotype-matched CT and VB, in bold when <0.05, Mann-Whitney *U* test, N = 9–10 mice/group. See also Table S4. (B) Effect of WBV on local femoral cortical bone thickness in $OPN^{-/-}$ and $BSP^{-/-}$ mice. The graphs show the percent variation of VB vs CT in each sector (mean ± SD), for $OPN^{-/-}$ (yellow bars) and $BSP^{-/-}$ mice (red bars). *: $p < 0.05$, **: $p < 0.01$, ***: $p < 0.001$ vs CT, Fisher's *t*-test, N = 9–10 mice/group. The schematics on the right summarize the targeted effects of WBV on $OPN^{-/-}$ (loss in yellow areas) and $BSP^{-/-}$ cortical bone (gain in red areas).

3.4. Whole body vibration induces opposite cellular responses in $OPN^{-/-}$ and $BSP^{-/-}$ cortical bones

WBV did not affect significantly formation and resorption parameters in endocortical and periosteal surfaces of WT and DKO mice (Fig. 5A). Vibrated $OPN^{-/-}$ mice showed a decrease in endocortical formation (Ec.BFR/BPm: −54 %, Figs. 5A, 6; Table S4) and in periosteal MAR (−21 %, Figs. 5B, 6), in line with a trend towards decreased OCN expression ($p = 0.062$, Table S5). This went with an increase of endocortical resorption in $OPN^{-/-}$ mice under WBV (Ec.Oc.Pm/BPm: +95 %, Figs. 5A, 6). Vibrated $BSP^{-/-}$ mice increased bone formation activity both on the endocortical (Figs. 5A, 6) and periosteal surfaces (Figs. 5B, 6) with additionally a drop in sclerostin (SCLN) expression (Fig. 5C). $BSP^{-/-}$ mice also showed a decrease in periosteal Oc.Pm/BPm (−68 %, Figs. 5B, 6A) with a drop in Receptor activator of nuclear factor kappa-B ligand (RANKL) and Cathepsin K (CATH-K) expression in cortical bone under WBV (Fig. 5C).

4. Discussion

The rapid and transient increase in gene expression of OPN and BSP under mechanical stimulation has been amply documented (Kreke et al.,

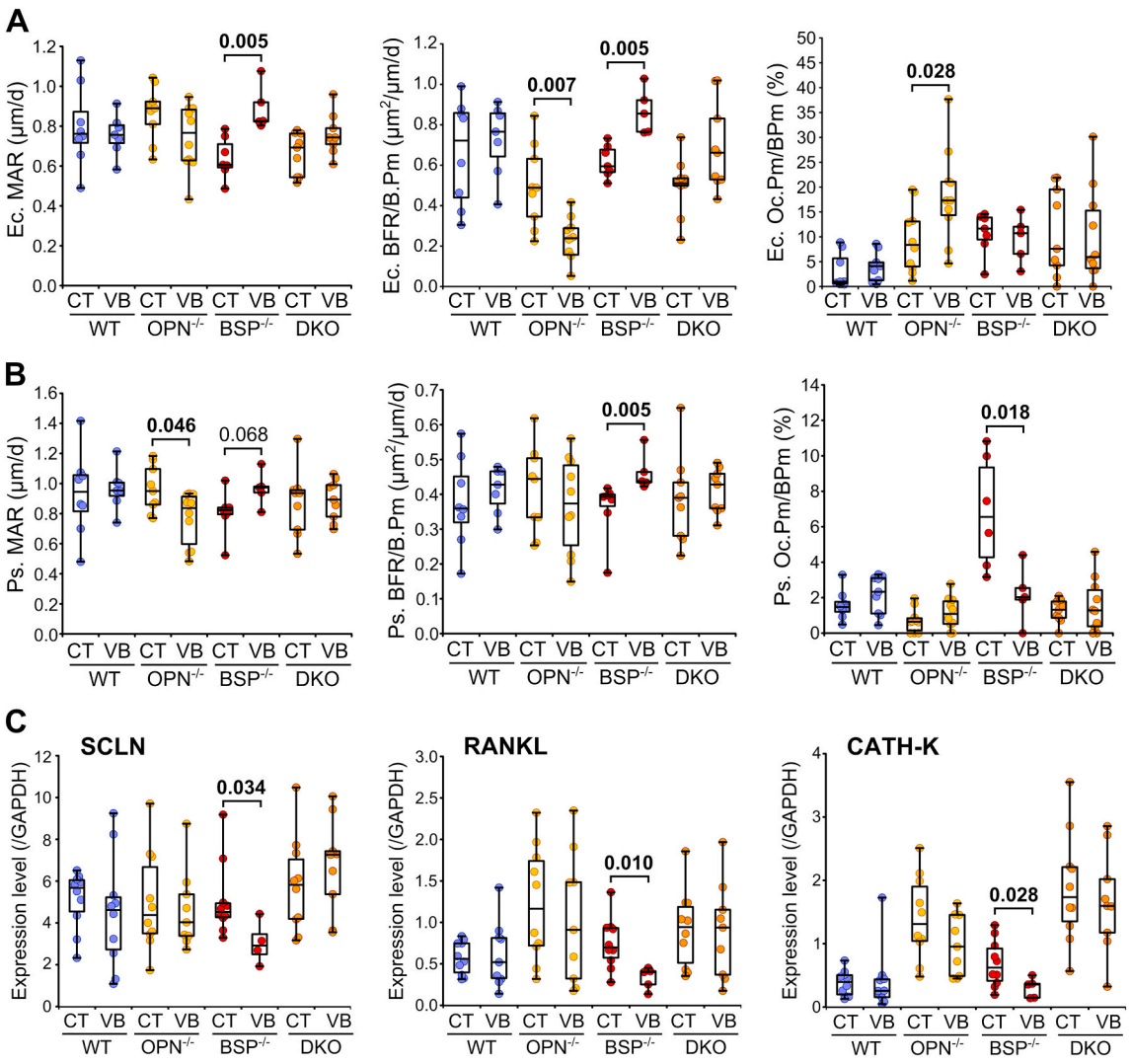

Fig. 5. Effect of WBV on cortical cellular activities in the femur of WT, OPN$^{-/-}$, BSP$^{-/-}$ and DKO mice. (A) endocortical and (B) persioteal MAR, BFR/BPm and Oc.Pm/BPm in the cortical bone of control (CT) and vibrated (VB) mice. (C) Marker mRNA expression in femur cortical bone of WT, OPN−/−, BSP−/− and DKO mice. Values are given as ratio to GAPDH. The graphs gives p values between genotype-matched CT and VB, in bold when <0.05, Mann-Whitney U test, N = 4–10 mice/group. See also Table S4.

2005; Mitsui et al., 2005; Terai et al., 1999; Yu et al., 2009; Zhou et al., 2015). The variations in expression of either protein observed in the different genotypes under both challenges (Tables S3, S5) reflect here long term temporal kinetics, independent of this early response. As far as we know, no studies to date tested BSP-deficient mice under mechanical stimulation. Moreover, due to the complex functional interactions between OPN and BSP that we highlighted in previous studies (Bouleftour et al., 2015, 2019; Granito et al., 2015), the DKO model was critical here to assess the interplay between OPN and BSP under mechanical challenge.

The bone phenotypes of the 4 mouse lines used in this study has been extensively described (Bouleftour et al., 2016, 2019; Malaval et al., 2008). Briefly, the trabecular BV/TV of the distal femur in BSP$^{-/-}$ and OPN$^{-/-}$ mice is similar to WT at 2 months (the start of our experiments) and increases to values higher than WT (~+25 %) in mature, 4 month-old mice. DKO mice have lower values (−30 %) at 2 months that reach WT values by 4 months (Bouleftour et al., 2019). At the end of our experiments (3.5 months of age), OPN$^{-/-}$ and BSP$^{-/-}$ values were already higher than WT (only in trend for BSP$^{-/-}$ femur in the 1G group, Tables S2, S4). BSP$^{-/-}$ mice are characterized by thinner cortices than WT, while OPN$^{-/-}$ cortical bone is thicker (Bouleftour et al., 2019). DKO cortical bone has the same average Ct.Th as WT in the midshaft area assessed, but presents remarkable macro-porosities in the posterior part of the midshaft (Bouleftour et al., 2019). This was observed at the end of our experiments (Tables S2, S4) with, in addition, no difference between genotypes in biomechanically relevant parameters such as pMOI, Imax, Imin, Imax/Cmax and Imin/Cmin (Table S4).

The present study shows that the single extinction of OPN or BSP affects the response of bone to mechanical stimulation in opposite ways, while their concomitant absence results in no structural effects. These findings were made with two different mechanical stress protocols, which mainly affect trabecular bone (HG, (Gnyubkin et al., 2015)) or mainly target cortical bone (WBV, (Gnyubkin et al., 2016)).

Our group previously reported an increase of trabecular BV/TV under HG in C57Bl/6 mice, associated with a drop of osteoclast surfaces (Gnyubkin et al., 2015), that we confirm here on WT 129sv/CD1 outbred mice, in which increased bone formation marker expression also suggests a stimulation of osteogenesis (Fig. 3D). This contrasts with the response of OPN$^{-/-}$ mice which show a drop in trabecular BV/TV with increased turnover under HG. Intriguingly, OPN$^{-/-}$ was the only genotype to increase osteoclast surfaces under both protocols (HG and WBV) in all the bone compartments investigated by histomorphometry. Historically, OPN$^{-/-}$ mice have been shown to be resistant to bone loss induced by hindlimb unloading (tail suspension) or ovariectomy, in part

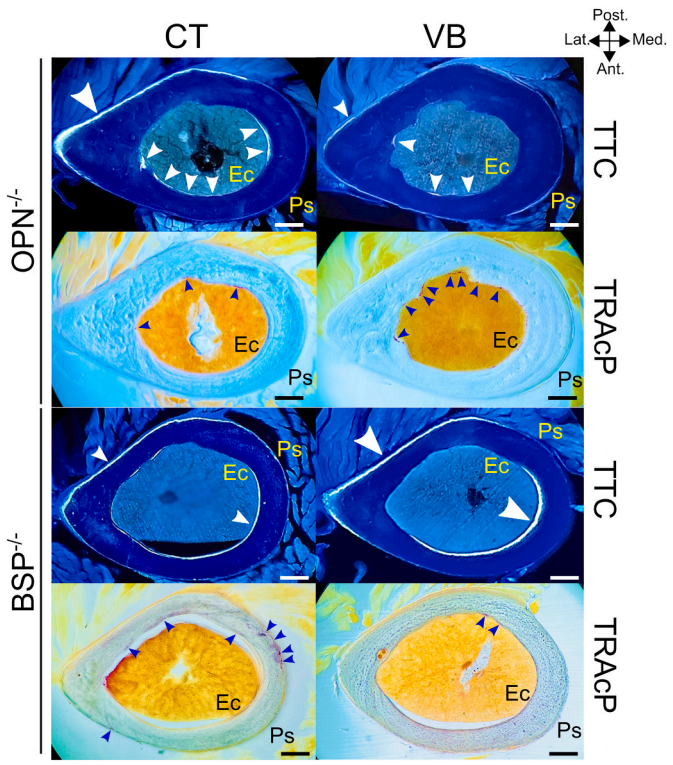

Fig. 6. Representative images of $OPN^{-/-}$ and $BSP^{-/-}$ femoral cortical bone dynamics under WBV. Tetracycline labeling and TRAcP staining of osteoclasts of $OPN^{-/-}$ and $BSP^{-/-}$ cortical bone from control (CT) and vibrated (VB) mice; bars = 250 μm; white arrows: formation surfaces, blue arrows: osteoclast surfaces. Abbreviations: TTC: tetracycline; TRAcP: tartrate-resistant acid phosphatase; Ec: endocortical surface; Ps: periosteal surface.

due to impaired stimulation of osteoclast activity (Ishijima et al., 2001; Yoshitake et al., 1999). Our results indicate that the defect in $OPN^{-/-}$ osteoclast sensitivity can be rescued by mechanical stress. All this suggests that OPN has a pivotal role in the sensitivity and/or response of osteoclasts to variations in the mechanical environment. That $OPN^{-/-}$ mice also display a decrease of bone formation parameters in the cortical compartment under WBV indicates that the mutation also affects the osteoblast response. In line with the delayed formation activity under tensile mechanical stress in $OPN^{-/-}$ calvarial sutures reported by (Morinobu et al., 2003), our results suggest a mechanoprotective function for OPN in bone. Interestingly such a role has been described in the kidney, where OPN protects against the deleterious mechanical effects of glomerular hypertension on podocytes through its attachment to the αV integrin (Endlich et al., 2002; Schordan et al., 2011). Similarly, bone cells grown from $OPN^{-/-}$ long bones display a defective production of nitric oxide (NO), a mediator of osteoblast mechanotransduction (Qin et al., 2020), under pulsatile fluid flow (Denhardt et al., 2001).

In $BSP^{-/-}$ mice, the increase in trabecular BV/TV under HG concerned both femur and vertebra. Of note, trabecular BV/TV is higher than WT at both sites in 1G $BSP^{-/-}$ mice, indicating that the response to HG is not a mere adjustment of bone mass to the new mechanical environment. Under HG, $BSP^{-/-}$ mice increased their trabecular BFR/BS, and molecular data from the endosteal (including the trabecular) compartment showed a higher ERα expression. ERα role in mechanotransduction has been described as pro-osteogenic (Khalid and Krum, 2016), inducing osteoblastic maturation through the upregulation of mitochondrial cytochrome *c* oxidase (COX) 1 mRNA and more globally by improving cellular ATP synthesis (Galea et al., 2013; Wu et al., 2020).

WBV did not accelerate the cortical growth of our WT mice, in contrast to (Gnyubkin et al., 2016), likely because of the different age of the animals at the start of the experiment (2 months vs 7 weeks in (Gnyubkin et al., 2016)), as well as the different genetic backgrounds. However, and in contrast to $OPN^{-/-}$, $BSP^{-/-}$ mice under WBV did show an increase in cortical thickness. Surprisingly, VB $BSP^{-/-}$ mice, in addition to an increased global bone formation in cortical bone, associated with a drop of sclerostin expression, also decreased their periosteal resorption activity, which at baseline (in $BSP^{-/-}$ CT) is the highest of all 4 genotypes. This correlated with decreased cortical expression of RANKL and CathK. We have previously shown that in contrast to WT, $BSP^{-/-}$ mice do not increase cortical thickness under intermittent Parathyroid Hormone (iPTH) administration (Wade-Gueye et al., 2010). WBV is indeed the only known experimental challenge to increase Ct.Th in $BSP^{-/-}$ mice, suggesting a specific role of BSP in the skeletal response to mechanical stimuli.

Taking into account all the data obtained in HG and WBV, the contrast between $OPN^{-/-}$ mice losing and $BSP^{-/-}$ mice gaining bone is further emphasized by the fact that DKO mice did not display any significant structural change under either protocol. Also, DKO mice showed little or no change in cellular parameters, suggesting that the concomitant absence of OPN and BSP induces a relative insensitivity of osteoblast and osteoclast responses under mechanical stimulation. Clearly, the interactions between OPN and BSP appear to be a key element in the skeletal response to mechanical stress.

We used only young male mice in this work, and extending the experiments to females would be required to assess a sex bias in the effect of OPN and BSP deletion during mechanical stress. Also the effect of mouse aging on the bone response of the different genotypes remains to be evaluated. Similar experiments on mice with deletions targeted to specific cell types (osteoblasts via Ocn-cre, osteoclasts via Cath-K-cre or osteocytes via DMP1-cre) would be a logical follow-up to our observations and may advance the unraveling of the cellular mechanisms involved.

In summary, under two different whole body mechanical stress protocols, targeting distinct bone compartments, $BSP^{-/-}$ mice gain bone mass while $OPN^{-/-}$ mice lose bone. Absence of both proteins (DKO) leads to insensitivity to mechanical stress, at least in terms of final outcome and with the challenges used in this work. These results suggest that interplay between OPN and BSP is a key element of skeletal adaptation to mechanical stimulation.

Funding

The "Agence Nationale de la Recherche" (grants ANR-13-BSV1-0010-01 "Mouse_Kosto" to LM), the "Institut National de la Santé et de la Recherche Médicale" (INSERM), the "Université Jean Monnet" of Saint Etienne, and the "Ministère de l'Enseignement supérieur, de la Recherche et de l'Innovation" (PhD scholarship for Mathieu Maalouf).

CRediT authorship contribution statement

M. Maalouf: Conceptualization, Methodology, Validation, Formal analysis, Investigation, Resources, Writing – original draft, Writing – review & editing, Visualization. **H. Çinar:** Methodology, Validation, Formal analysis, Investigation. **W. Bouleftour:** Resources. **M. Thomas:** Methodology, Validation, Investigation, Data curation. **A. Vanden-Bossche:** Methodology, Investigation, Resources. **N. Laroche:** Investigation. **M.T. Linossier:** Methodology. **S. Peyroche:** Investigation. **M.H. Lafage-Proust:** Writing – review & editing. **L. Vico:** Resources, Writing – review & editing, Funding acquisition. **A. Guignandon:** Conceptualization, Writing – review & editing, Supervision. **L. Malaval:** Conceptualization, Methodology, Validation, Formal analysis, Investigation, Resources, Writing – review & editing, Visualization, Supervision, Project administration, Funding acquisition.

Declaration of competing interest

The authors declare that they have no known competing financial

interests or personal relationships that could have appeared to influence the work reported in this paper.

Data availability

Data will be made available on request.

Acknowledgements

The small animal centrifuge is an open facility of the Centre National d'Etudes Spatiales (CNES, Paris, France). The authors thank the staff of the PLEXAN facility for skillful technical assistance, Dr. Myriam Normand and Dr. Bernard Roche (U1059, LBTO) for advice on statistics, Elisa Dalix for help with RT-qPCR and Dr. Laura Peurière for help in HG mice sample harvesting.

Appendix A. Supplementary data

Supplementary data to this article can be found online at https://doi.org/10.1016/j.bonr.2022.101621.

References

Bouleftour, W., Bouet, G., Granito, R.N., Thomas, M., Linossier, M.-T., Vanden-Bossche, A., Aubin, J.E., Lafage-Proust, M.-H., Vico, L., Malaval, L., 2015. Blocking the expression of both bone sialoprotein (BSP) and osteopontin (OPN) impairs the anabolic action of PTH in mouse calvaria bone: either BSP or OPN is required for PTH action. J. Cell. Physiol. 230 (3), 568–577. https://doi.org/10.1002/jcp.24772.

Bouleftour, W., Juignet, L., Bouet, G., Granito, R.N., Vanden-Bossche, A., Laroche, N., Aubin, J.E., Lafage-Proust, M.-H., Vico, L., Malaval, L., 2016. The role of the SIBLING, bone sialoprotein in skeletal biology—contribution of mouse experimental genetics. Matrix Biol. 52–54, 60–77. https://doi.org/10.1016/j.matbio.2015.12.011.

Bouleftour, W., Juignet, L., Verdière, L., Machuca-Gayet, I., Thomas, M., Laroche, N., Vanden-Bossche, A., Farlay, D., Thomas, C., Gineyts, E., Concordet, J.P., Renaud, J. B., Aubert, D., Teixeira, M., Peyruchaud, O., Vico, L., Lafage-Proust, M.H., Follet, H., Malaval, L., 2019. Deletion of OPN in BSP knockout mice does not correct bone hypomineralization but results in high bone turnover. Bone 120, 411–422. https://doi.org/10.1016/j.bone.2018.12.001.

Bouxsein, M.L., Boyd, S.K., Christiansen, B.A., Guldberg, R.E., Jepsen, K.J., Müller, R., 2010. Guidelines for assessment of bone microstructure in rodents using micro–computed tomography. J. Bone Miner. Res. 25 (7), 1468–1486. https://doi.org/10.1002/jbmr.141.

Denhardt, D.T., Burger, E.H., Kazanecki, C., Krishna, S., Semeins, C.M., Klein-Nulend, J., 2001. Osteopontin-deficient bone cells are defective in their ability to produce NO in response to pulsatile fluid flow. Biochem. Biophys. Res. Commun. 288 (2), 448–453. https://doi.org/10.1006/bbrc.2001.5780.

Endlich, N., Sunohara, M., Nietfeld, W., Wolski, E.W., Schiwek, D., Kränzlin, B., Gretz, N., Kriz, W., Eickhoff, H., Endlich, K., 2002. Analysis of differential gene expression in stretched podocytes: osteopontin enhances adaptation of podocytes to mechanical stress. FASEB J. 16 (13), 1850–1852. https://doi.org/10.1096/fj.02-0125fje.

Fisher, L.W., Fedarko, N.S., 2003. Six genes expressed in bones and teeth encode the current members of the SIBLING family of proteins. Connect. Tissue Res. 44 (1), 33–40. https://doi.org/10.1080/03008200390152061.

Galea, G.L., Meakin, L.B., Sugiyama, T., Zebda, N., Sunters, A., Taipaleenmaki, H., Stein, G.S., van Wijnen, A.J., Lanyon, L.E., Price, J.S., 2013. Estrogen receptor α mediates proliferation of osteoblastic cells stimulated by estrogen and mechanical strain, but their acute Down-regulation of the wnt antagonist sost is mediated by estrogen receptor β *. J. Biol. Chem. 288 (13), 9035–9048. https://doi.org/10.1074/jbc.M112.405456.

Ganss, B., Kim, R.H., Sodek, J., 1999. Bone sialoprotein. Crit. Rev. Oral Biol. Med. 10 (1), 79–98. https://doi.org/10.1177/10454411990100010401.

Gnyubkin, V., Guignandon, A., Laroche, N., Vanden-Bossche, A., Malaval, L., Vico, L., 2016. High-acceleration whole body vibration stimulates cortical bone accrual and increases bone mineral content in growing mice. J. Biomech. 49 (9), 1899–1908. https://doi.org/10.1016/j.jbiomech.2016.04.031.

Gnyubkin, V., Guignandon, A., Laroche, N., Vanden-Bossche, A., Normand, M., Lafage-Proust, M.-H., Vico, L., 2015. Effects of chronic hypergravity: from adaptive to deleterious responses in growing mouse skeleton. J. Appl. Physiol. 119 (8), 908–917. https://doi.org/10.1152/japplphysiol.00364.2015.

Granito, R.N., Bouleftour, W., Sabido, O., Lescale, C., Thomas, M., Aubin, J.E., Goodhardt, M., Vico, L., Malaval, L., 2015. Absence of bone sialoprotein (BSP) alters profoundly hematopoiesis and upregulates osteopontin: lack of BSP alters bone marrow composition. J. Cell. Physiol. 230 (6), 1342–1351. https://doi.org/10.1002/jcp.24877.

Ishijima, M., Rittling, S.R., Yamashita, T., Tsuji, K., Kurosawa, H., Nifuji, A., Denhardt, D. T., Noda, M., 2001. Enhancement of osteoclastic bone resorption and suppression of osteoblastic bone formation in response to reduced mechanical stress do not occur in the absence of osteopontin. J. Exp. Med. 193 (3), 399–404.

Khalid, A.B., Krum, S.A., 2016. Estrogen receptors alpha and beta in bone. Bone 87, 130–135. https://doi.org/10.1016/j.bone.2016.03.016.

Kreke, M.R., Huckle, W.R., Goldstein, A.S., 2005. Fluid flow stimulates expression of osteopontin and bone sialoprotein by bone marrow stromal cells in a temporally dependent manner. Bone 36 (6), 1047–1055. https://doi.org/10.1016/j.bone.2005.03.008.

Malaval, L., Wade-Guéye, N.M., Boudiffa, M., Fei, J., Zirngibl, R., Chen, F., Laroche, N., Roux, J.-P., Burt-Pichat, B., Duboeuf, F., Boivin, G., Jurdic, P., Lafage-Proust, M.-H., Amédée, J., Vico, L., Rossant, J., Aubin, J.E., 2008. Bone sialoprotein plays a functional role in bone formation and osteoclastogenesis. J. Exp. Med. 205 (5), 1145–1153. https://doi.org/10.1084/jem.20071294.

Mitsui, N., Suzuki, N., Maeno, M., Mayahara, K., Yanagisawa, M., Otsuka, K., Shimizu, N., 2005. Optimal compressive force induces bone formation via increasing bone sialoprotein and prostaglandin E2 production appropriately. Life Sci. 77 (25), 3168–3182. https://doi.org/10.1016/j.lfs.2005.03.037.

Morinobu, M., Ishijima, M., Rittling, S.R., Tsuji, K., Yamamoto, H., Nifuji, A., Denhardt, D.T., Noda, M., 2003. Osteopontin expression in osteoblasts and osteocytes during bone formation under mechanical stress in the calvarial suture in vivo. J. Bone Miner. Res. 18 (9), 1706–1715. https://doi.org/10.1359/jbmr.2003.18.9.1706.

Qin, Liu, W., Cao, H., Xiao, G., 2020. Molecular mechanosensors in osteocytes. Bone Res. 8 (1), 23. https://doi.org/10.1038/s41413-020-0099-y.

Schordan, S., Schordan, E., Endlich, K., Endlich, N., 2011. AV-integrins mediate the mechanoprotective action of osteopontin in podocytes. Am. J. Physiol. Ren. Physiol. 300 (1), F119–F132. https://doi.org/10.1152/ajprenal.00143.2010.

Sodek, J., Ganss, B., McKee, M.D., 2000. Osteopontin. Crit. Rev. Oral Biol. Med. 11 (3), 279–303. https://doi.org/10.1177/10454411000110030101.

Staines, K.A., MacRae, V.E., Farquharson, C., 2012. The importance of the SIBLING family of proteins on skeletal mineralisation and bone remodelling. J. Endocrinol. 214 (3), 241–255. https://doi.org/10.1530/joe-12-0143.

Terai, K., Takano-Yamamoto, T., Ohba, Y., Hiura, K., Sugimoto, M., Sato, M., Kawahata, H., Inaguma, N., Kitamura, Y., Nomura, S., 1999. Role of osteopontin in bone remodeling caused by mechanical stress. J. Bone Miner. Res. 14 (6), 839–849. https://doi.org/10.1359/jbmr.1999.14.6.839.

Wade-Gueye, N.M., Boudiffa, M., Laroche, N., Vanden-Bossche, A., Fournier, C., Aubin, J. E., Vico, L., Lafage-Proust, M.-H., Malaval, L., 2010. Mice lacking bone sialoprotein (BSP) lose bone after ovariectomy and display skeletal site-specific response to intermittent PTH treatment. Endocrinology 151 (11), 5103–5113. https://doi.org/10.1210/en.2010-0091.

Wu, G.-J., Chen, J.-T., Lin, P.-I., Cherng, Y.-G., Yang, S.-T., Chen, R.-M., 2020. Inhibition of the estrogen receptor alpha signaling delays bone regeneration and alters osteoblast maturation, energy metabolism, and angiogenesis. Life Sci. 258, 118195 https://doi.org/10.1016/j.lfs.2020.118195.

Yoshitake, H., Rittling, S.R., Denhardt, D.T., Noda, M., 1999. Osteopontin-deficient mice are resistant to ovariectomy-induced bone resorption. Proc. Natl. Acad. Sci. U. S. A. 96 (14), 8156–8160.

Yu, H., Ren, Y., Sandham, A., Ren, A., Huang, L., Bai, D., 2009. Mechanical tensile stress effects on the expression of bone sialoprotein in bovine cementoblasts. Angle Orthod. 79 (2), 346–352. https://doi.org/10.2319/011508-20.1.

Zhou, S., Zu, Y., Sun, Z., Zhuang, F., Yang, C., 2015. Effects of hypergravity on osteopontin expression in osteoblasts. PLOS ONE 10 (6), e0128846. https://doi.org/10.1371/journal.pone.0128846.